Diffraction of plane waves by a periodic array of nonlinear circular cylinders

Lijun Yuan*
College of Mathematics and Statistics, Chongqing Technology and Business University, Chongqing, China

Ya Yan Lu
Department of Mathematics, City University of Hong Kong, Hong Kong

It is well-known that standing waves, as special bound states in the radiation continuum, may exist on a periodic array of dielectric cylinders at a discrete set of frequencies, if the medium is linear. Recent numerical studies indicate that nonlinear standing waves could exist continuously with respect to the frequency on a periodic array of cylinders with a Kerr nonlinearity. In this paper, we study the diffraction of a normal incident plane wave by a periodic array of circular cylinders with a Kerr nonlinearity. Using a perturbation method and a highly accurate numerical method, we show that a plane incident wave may couple to a nonlinear standing wave, and in general, there are four different couplings leading to four asymmetric solutions in two pairs. The existence of these asymmetric solutions provides another example for the symmetry breaking phenomenon. Importantly, it seems that the asymmetric solutions (thus the symmetry breaking phenomenon) appear for incident waves of arbitrarily low intensity.

PACS numbers: 42.65.Hw,42.25.Fx,42.79.Dj

I. INTRODUCTION

The optical Kerr effect is responsible for many interesting nonlinear phenomena such as self-focusing and filamentation of laser beams, temporal and spatial solitons, optical bistability, symmetry breaking, etc. [1]. In particular, optical bistability [2–5] and symmetry breaking [6–10] are related to the existence of multiple solutions for the same incident wave, and have potential applications in all-optical switching [11, 12], filtering [13], etc. However, since the nonlinear coefficients of conventional dielectric materials are very small, most nonlinear phenomena related to the Kerr nonlinearity can only be observed for incident waves with a very high intensity or over a very long interaction length. These constrains put a serious limitation on applications of these nonlinear phenomena in nanophotonics, where the device size, the operating power, and operation time must all be extremely small. One possible approach to overcome these limitations is to enhance the nonlinear effect by microcavities [4, 14]. In that case, even when the incident wave is not so strong, the field in the microcavity is enhanced due to resonances, and the nonlinear phenomena such as optical bistability and symmetry breaking can be observed. However, there is still a minimum incident power or intensity for the appearance of these nonlinear phenomena, and it could be still too high when practical microcavities are used. In this paper, we show that the symmetry breaking phenomenon could occur in a simple periodic structure for incident plane waves with arbitrarily low intensity.

We consider a one-dimensional (1D) array of parallel and infinitely long dielectric cylinders surrounded by air. Such an array can be regarded as a two-dimensional (2D) periodic waveguide [15]. For linear cylinders, the array supports various guided modes that are invariant along the cylinder axes, propagate along the periodic direction, and decay exponentially in the transverse direction [16]. The guided modes typically exist below the lightline, that is, $\omega n_0/c < |\beta|$, where ω is the angular frequency, $n_0 = 1$ is the refractive index of air, c is the speed of light in vacuum, and β is the Bloch wavenumber (or propagation constant) of the guided mode. Notice that the guided modes below the lightline exist continuously with respect to the frequency, and ω and β are related to each other by the dispersion curves. Above the lightline is the continuum of radiation modes, thus, guided modes that do not radiate power are more difficult to find. Nevertheless, it is known that guided modes could exist above the lightline [17–24]. These modes are bound states in the radiation continuum, they correspond to eigenvalues in the continuous spectrum, and only exist as isolated points in the $\beta\omega$ plane. The special guided modes above the lightline with $\beta = 0$ are standing waves that do not propagate. For arrays with a reflection symmetry along the periodic direction, the existence of standing waves are well established [17, 21]. The existence of guided modes above the lightline is related to the non-uniqueness of the diffraction problem for incident plane waves [17, 21]. More precisely, if there is a guided mode above the lightline at (β, ω), then the boundary value problem for an incident plane wave with frequency ω and wavevector component β has no uniqueness. In addition, strong resonant effects may be observed for incident waves with a slightly different β [25, 26].

In a recent work [27], we found nonlinear standing waves (NSWs) on a periodic array of circular cylinders with a Kerr nonlinearity through rigorous numerical simulations using a highly accurate numerical method. The NSWs are special nonlinear bound states in the radiation continuum [28, 29]. They are solutions without any in-

* Corresponding author: ljyuan@ctbu.edu.cn

cident waves, are localized around the cylinders, and do not propagate along the array. Unlike the linear standing waves, the NSWs exist continuously with respect to the frequency, and their amplitudes vary with the frequency. Near the frequencies of the linear standing waves, there are NSWs with relatively small amplitudes. In this paper, we study the diffraction of a normal incident plane wave by a periodic array of nonlinear circular cylinders, and show that the incident wave may couple with the NSWs, so that the diffraction problem has multiple solutions for any given frequency. Importantly, an incident wave of arbitrarily small amplitude may couple to the NSWs, so that multiple solutions exist without any condition on the intensity of the incident wave. Due to the different symmetries between the incident wave and the NSWs, their coupling is a symmetry breaking phenomenon.

The rest of this paper is organized as follows. In Section II, we describe the problem and give a mathematical formulation. In Section III, we present some results on NSWs. In Section IV, a perturbation theory is developed for incident waves with small amplitudes. The main results on the nonlinear diffraction problem are presented in Section V. We conclude the paper with some discussion in Section 6.

II. FORMULATION

In Fig. 1, we show a periodic array of parallel and

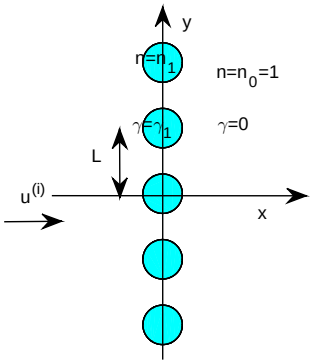

FIG. 1. A plane wave $u^{(i)}$ impinges on a periodic array of circular cylinders under the normal incidence.

infinitely long circular cylinders surrounded by air. In a Cartesian coordinate system $\{x, y, z\}$, the cylinders are parallel to the z axis, and the array is periodic in y with period L. The refractive index and the radius of the cylinders are n_1 and a, respectively, where $n_1 > 1$ and $a < L/2$. As shown in Fig. 1, the structure is symmetric with respect to both x and y axes. We assume that cylinders are made from a dielectric material with a Kerr nonlinearity.

For the E polarization and assuming the higher harmonics can be ignored, the nonlinear Maxwell's equations can be reduced to the following nonlinear Helmholtz equation [1, 3, 5, 30–32]:

$$\frac{\partial^2 u}{\partial x^2} + \frac{\partial^2 u}{\partial y^2} + k_0^2 \left(n^2 + \gamma |u|^2\right) u = 0, \tag{1}$$

where u is the z component of the electric field, $k_0 = \omega/c$ is the free space wavenumber, $n = n(x, y)$ is the refractive index function, $\gamma = \frac{3}{4}\chi^{(3)}$ is the nonlinear coefficient satisfying $\gamma = \gamma_1 > 0$ in the cylinders and $\gamma = 0$ outside the cylinders, and $\chi^{(3)}$ is an element of the third order nonlinear susceptibility tensor. The normal incident plane wave is given by

$$u^{(i)}(x, y) = A^{(i)} e^{\mathrm{i}k_0 n_0 (x + L/2)}, \tag{2}$$

where $A^{(i)}$ is the amplitude. Our objective is to analyze the diffraction of normal incident plane waves by this array of nonlinear cylinders.

Since the structure is periodic in y and the incident wave is invariant in y, we consider solutions that are also periodic in y. Therefore, u satisfies

$$u(x, y + L) = u(x, y). \tag{3}$$

Meanwhile, the solution can be expanded in plane waves for $|x| > a$. For the transmitted and reflected waves, the wave vectors are (α_m, β_m) and $(-\alpha_m, \beta_m)$, respectively, where m is any integer,

$$\beta_m = \frac{2\pi m}{L}, \quad \alpha_m = \sqrt{k_0^2 n_0^2 - \beta_m^2}. \tag{4}$$

Comparing the plane wave expansions of u and $\partial u/\partial x$, we can write down rigorous nonlocal boundary conditions at $x = \pm L/2$ [33]. If we define a linear operator $\mathcal{T}$ by

$$\mathcal{T} e^{\mathrm{i}\beta_m y} = \mathrm{i}\alpha_m e^{\mathrm{i}\beta_m y} \quad \text{for} \quad m = 0, \pm 1, \pm 2, \ldots \tag{5}$$

then the boundary conditions are

$$\frac{\partial u}{\partial x} = -\mathcal{T} u + 2\mathrm{i}\alpha_0 A^{(i)}, \quad x = -\frac{L}{2}, \tag{6}$$

$$\frac{\partial u}{\partial x} = \mathcal{T} u, \quad x = \frac{L}{2}. \tag{7}$$

The term $2\mathrm{i}\alpha_0 A^{(i)}$ in the right hand side of Eq. (6) is related to the incident wave. Because of the boundary conditions (3), (6) and (7), Eq. (1) only needs to be solved on the square

$$S = \{(x, y) \ : \ |x| < L/2, \ |y| < L/2\}. \tag{8}$$

Due to the nonlinearity, Eq. (1) can only be solved by an iterative method. We use an efficient iterative method and a highly accurate discretization scheme to find the solutions of Eq. (1). The numerical methods are briefly described in Appendix A.

III. STANDING WAVES

For the periodic array shown in Fig. 1, a guided mode is a solution of Eq. (1) given as

$$u(x,y) = \phi(x,y)e^{\mathrm{i}\beta y}, \tag{9}$$

where β is the Bloch wavenumber (or propagation constant) of the mode, ϕ is periodic in y with period L and decays exponentially to zero as $|x| \to \infty$. For linear cylinders, i.e., if $\gamma = 0$, guided modes exist continuously below the light line (that is, $k_0 n_0 < |\beta|$), and ω is related to β by dispersion curves [15, 16]. Standing waves are special guided modes with $\beta = 0$. Away from the cylinders, a standing wave can be expanded in plane waves as

$$\phi(x,y) = \begin{cases} \sum\limits_m b_m^- \, e^{\mathrm{i}[\beta_m y - \alpha_m (x+L/2)]}, & x < -a, \\ \sum\limits_m b_m^+ \, e^{\mathrm{i}[\beta_m y + \alpha_m (x-L/2)]}, & x > a. \end{cases} \tag{10}$$

where α_m and β_m are given in Eq. (4), and $b_m^{\pm}$ are unknown coefficients. If the frequency satisfies $\omega L/(2\pi c) < 1$ (for $n_0 = 1$), then α_0 is positive and all other α_m for $m \neq 0$ are pure imaginary. In that case, to ensure that ϕ decays to zero as $|x| \to \infty$, we only need the condition $b_0^{\pm} = 0$. Notice that if ϕ is an odd function of y, i.e. $\phi(x,y) = -\phi(x,-y)$, then this condition is automatically satisfied.

For arrays with a reflection symmetry in the periodic direction, the existence of antisymmetric linear standing waves (i.e., odd functions in y) are well established [17–21, 23, 24]. The linear standing waves only exist at a discrete set of frequencies. For an array of circular cylinders with refractive index $n_1 = 2.5$ and radius $a = 0.3L$, there are two antisymmetric linear standing waves within the frequency interval $\omega L/(2\pi c) < 1$. These two modes appears at $\omega L/(2\pi c) = 0.5502$ and 0.7800, respectively.

In a recent work [27], we analyzed NSWs on periodic arrays of circular cylinders. Unlike the linear standing waves, the NSWs exist continuously with respect to the frequency and their amplitudes depend on the frequency. For the array with $n_1 = 2.5$, $a = 0.3L$ and $\gamma_1 > 0$, the amplitude-frequency relations of the first a few NSWs are shown in Fig.2. The amplitude A is defined as $\max|\phi(x,y)|$, and it is inversely proportional to $\sqrt{\gamma_1}$. Since γ_1 is extremely small, the amplitudes are typically very large. However, two NSWs are directly linked to the linear standing waves. Their amplitudes tend to zero as ω approaches the corresponding frequencies of the linear standing waves. Notice that the NSWs can have arbitrary phases. If $\phi(x,y)$ is a NSW, then so is $C\phi(x,y)$ where C is a complex number with unit magnitude. For $\gamma_1 = 2 \times 10^{-12}$ m^2/V^2, the electric field patterns of the first three NSWs at frequency $\omega L/(2\pi c) = 0.53$, corresponding to points A, B and C in Fig. 2, are shown in Fig. 3. These NSWs are odd functions of y, and they vanish on horizontal lines at $y = 0$ and $y = \pm L/2$.

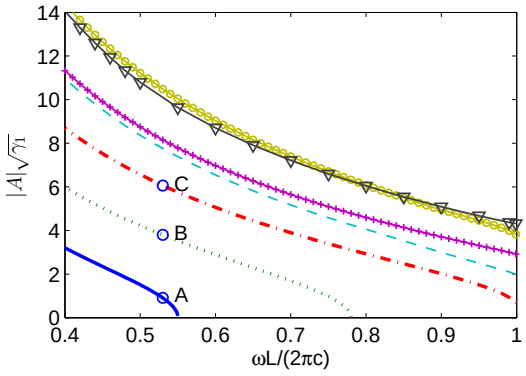

FIG. 2. Amplitude-frequency relations of seven nonlinear standing waves on a periodic array of circular cylinders with a Kerr nonlinearity.

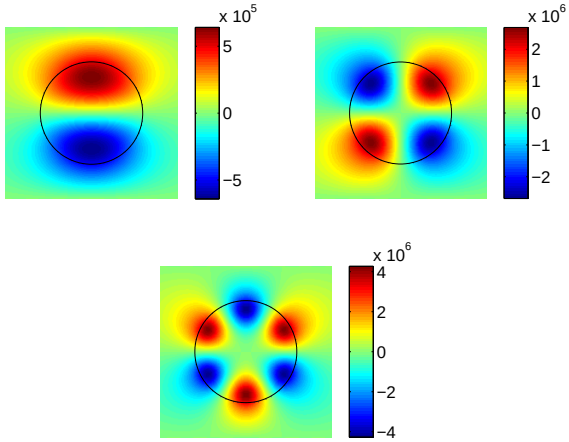

FIG. 3. Electric field patterns of the nonlinear standing waves at frequency $\omega L/(2\pi c) = 0.53$ corresponding to points A, B and C in Fig. 2 .

IV. PERTURBATION ANALYSIS

Nonlinear wave phenomena such as optical bistability and symmetry breaking are related to the existence of multiple solutions for the same incident wave, but they seem to appear only when the power or intensity of the incident wave is sufficiently high. This is true even when the nonlinear effect is enhanced by resonant cavities. In this and the next sections, we show that multiple solutions related to the symmetry breaking phenomenon can appear for incident waves of arbitrarily low intensity. Of course, this is only true for the ideal infinite periodic structure. The multiple solutions are the consequence of nonlinear coupling between the incident wave and the NSWs. In the following, we analyze the coupled solutions by a perturbation method.

In Section 2, we formulated the nonlinear diffraction problem on square S for governing equation (1) with boundary conditions (3), (6) and (7). Let $\delta = A^{(i)}/A$

be the ratio of the amplitudes of the incident plane wave and a NSW $\phi(x,y)$, we assume δ is small and seek the solution in a power series of δ:

$$u = C\left[\phi + A\left(\delta\phi_1 + \delta^2\phi_2 + ...\right)\right], \tag{11}$$

where C is an unknown complex number satisfying $|C| = 1$. Substituting Eq. (11) into Eq. (1), and gathering terms of equal powers of δ, we obtain

$$\mathcal{L}\phi + k_0^2\gamma|\phi|^2\phi = 0, \tag{12}$$
$$\mathcal{L}\phi_1 + k_0^2\gamma\left(2|\phi|^2\phi_1 + \phi^2\bar{\phi}_1\right) = 0, \tag{13}$$
$$\mathcal{L}\phi_2 + k_0^2\gamma\left(2|\phi|^2\phi_2 + \phi^2\bar{\phi}_2 + 2A\phi|\phi_1|^2 + A\bar{\phi}\phi_1^2\right) = 0, \tag{14}$$

where $\bar{\phi}$ is the complex conjugate of ϕ and $\mathcal{L}$ is given by

$$\mathcal{L} = \partial_x^2 + \partial_y^2 + k_0^2 n^2(x,y). \tag{15}$$

Substituting Eq. (11) into the boundary conditions (6) and (7), we obtain

$$\partial_x\phi = \pm\mathcal{T}\phi, \qquad x = \pm L/2, \tag{16}$$
$$\partial_x\phi_1 = \mathcal{T}\phi_1, \qquad x = L/2, \tag{17}$$
$$\partial_x\phi_1 = -\mathcal{T}\phi_1 + 2\mathrm{i}\alpha_0\bar{C}, \quad x = -L/2, \tag{18}$$
$$\partial_x\phi_2 = \pm\mathcal{T}\phi_2, \qquad x = \pm L/2, \tag{19}$$

where $\mathcal{T}$ is defined in Section 2. In addition, ϕ, ϕ_1 and ϕ_2 must all satisfy the periodic condition (3).

Equation (12) and boundary condition (16) for ϕ are not new. For any given C, ϕ_1 can be solved from Eqs. (13), (17) and (18). To determine C, we multiply Eq. (14) by $\bar{\phi}$ and integrate the result on S. After an integration by parts and some calculations on the boundary of S given in Appendix B, we obtain

$$\int_D \gamma|\phi|^2\left(\bar{\phi}\phi_2 + \phi\bar{\phi}_2 + 2A|\phi_1|^2\right)\mathrm{d}x\mathrm{d}y + A\int_D \gamma\bar{\phi}^2\phi_1^2\,\mathrm{d}x\mathrm{d}y = 0, \tag{20}$$

where D is the disk of radius a. Since $\gamma = \gamma_1$ in D and γ_1 is a constant, the imaginary part of Eq. (20) gives

$$\mathrm{Im}\left(\int_D \bar{\phi}^2\phi_1^2\,\mathrm{d}x\mathrm{d}y\right) = 0. \tag{21}$$

In Appendix B, we show that the above condition is also a direct consequence of the power balance law, namely, the incident power should equal to the total of reflected and transmitted powers.

Since ϕ_1 depends on C, Eq. (21) is actually a nonlinear equation for C. Let $C = \exp(\mathrm{i}d)$ for a real $d \in (-\pi, \pi]$, it is shown in Appendix B that $\phi_1 = \cos(d)\psi + \sin(d)\varphi$, where ψ and φ are independent of C, and satisfy (13), (17) and conditions similar to (18). This leads to real numbers θ_* and K depending on ϕ, ψ and φ, such that

$$\sin(2d + \theta_*) = K. \tag{22}$$

If it clear that Eq. (22) has four, two or zero solutions in $(-\pi, \pi]$, for $|K| < 1$, $|K| = 1$ or $|K| > 1$, respectively. More details are given in Appendix B.

V. NUMERICAL RESULTS

In this section, we show numerical solutions of the nonlinear diffraction problem for an array of circular cylinders with $n_1 = 2.5$, $a = 0.3L$ and $\gamma_1 = 2\times10^{-12}\,\mathrm{m}^2/\mathrm{V}^2$. For the coordinate system shown in Fig. 1, the structure and the incident wave have a reflection symmetry with respect to the x axis, but the diffraction problem can have both symmetric solutions (even functions of y) or asymmetric solutions. In Fig. 4, we show a symmetric solution for normalized frequency $\omega L/(2\pi c) = 0.53$ and incident amplitude $A^{(i)} = 10^3\,\mathrm{V/m}$. It is clear that $u(x,y)$ is an even function of y, and its magnitude is on the same order as $A^{(i)}$.

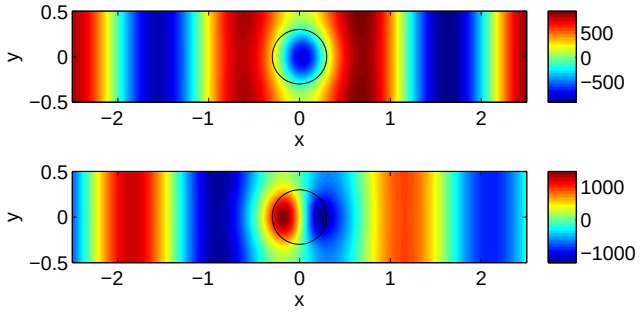

FIG. 4. Real (top) and imaginary (bottom) parts of u for the symmetric solution of the nonlinear diffraction problem at $\omega L/(2\pi c) = 0.53$ and $A^{(i)} = 10^3\,\mathrm{V/m}$.

The asymmetric solutions are those coupled to the NSWs. They are neither symmetric nor antisymmetric (odd functions of y), and they appear in pairs. If $u(x,y)$ is an asymmetric solution, then $u(x,-y)$ is also a solution. In most cases, for a fixed incident wave, there are four asymmetric solutions coupled to each NSW. The perturbation theory developed in Section 4 allows us to determine the coefficient C or its polar angle d. The pair $u(x,y)$ and $u(x,-y)$ are related to C and $-C$, respectively. In Fig. 5, we show d as functions of the frequency for the first three NSWs. The three panels in Fig. 5 correspond to the NSWs marked with A, B and C in Fig. 2, respectively. The solid red and dashed blue curves represent two different values of d. Each d gives rise to a pair of coefficients $C = \pm e^{\mathrm{i}d}$. In general, there are two different values of d for each NSW, but the solid red and dashed blue curves in Fig. 5 can intersect. For the third NSW, there is a frequency interval $(0.504, 0.52)$ in which coefficient C does not exist. In Table I, we list the values of C for the first three NSWs at frequency $\omega L/(2\pi c) = 0.53$, corresponding exactly to points A, B and C in Fig. 2.

The perturbation theory is derived under the assumption that the incident amplitude $A^{(i)}$ is much smaller than the amplitude A of a NSW ϕ. For a given $A^{(i)}$, we can find the asymmetric solution numerically using $C\phi$ or $C(\phi + A\delta\phi_1)$ as the initial guess. For the iterations, we use the modified Newton's method given in

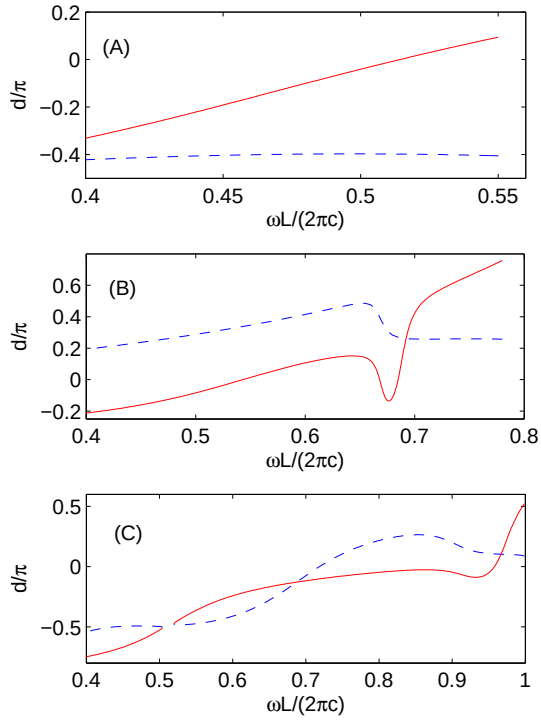

FIG. 5. Frequency dependence of polar angle d for coefficient $C = e^{id}$ in the perturbation theory. The panels (A), (B) and (C) correspond to the three lowest NSWs shown in Fig. 2.

NSW	Coefficient C	
A	$\pm(0.9910 + 0.1340\mathrm{i})$,	$\pm(0.3084 - 0.9513\mathrm{i})$
B	$\pm(0.9965 - 0.0832\mathrm{i})$,	$\pm(0.5297 + 0.8482\mathrm{i})$
C	$\pm(0.0544 - 0.9985\mathrm{i})$,	$\pm(0.2194 - 0.9756\mathrm{i})$

TABLE I. Coefficient C of the perturbation theory for three NSWs marked as A, B and C in Fig. 2.

Eq. (26). For $\omega L/(2\pi c) = 0.53$ and $A^{(i)} = 10^3\,\mathrm{V/m}$, we calculate two asymmetric solutions for each NSW. In Fig. 6, we show the two solutions coupled to the first NSW for $C = 0.9910 + 0.1340\mathrm{i}$ and $C = 0.3084 - 0.9513\mathrm{i}$, respectively. Since the amplitude of the NSW is around $6 \times 10^5\,\mathrm{V/m}$, and it is is much larger than $A^{(i)}$, the solutions are dominated by the NSW. To see more clearly the wave field away from the cylinders, we limit the field values from -1.5×10^3 to $1.5 \times 10^3\,\mathrm{V/m}$. It can be seen that away from the cylinders the field is dominated by plane waves propagating along the x axis, but around the cylinders, the field pattern looks like the one shown in Fig. 3. As mentioned earlier, there are two more asymmetric solutions associated with the NSW, and they are the mirror reflections (with respect to the x axis) of the two solutions obtained.

We have also calculated asymmetric solutions coupled to the second and third NSWs. In Fig. 7, we show four solutions. The first two panels show solutions coupled to the second NSW for $C = 0.9965 - 0.0832\mathrm{i}$ and $C = 0.5297 + 0.8482\mathrm{i}$, respectively. The third and fourth panels correspond to the third NSW with $C = 0.0544 - 0.9985\mathrm{i}$ and $C = 0.2194 - 0.9756\mathrm{i}$, respectively. The field values are also limited from -1.5×10^3 to $1.5 \times 10^3\,\mathrm{V/m}$.

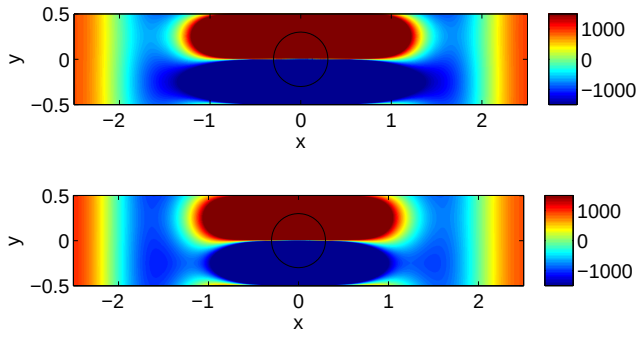

FIG. 6. Wave field patterns (real part of u) of two asymmetric solutions coupled to the first NSW.

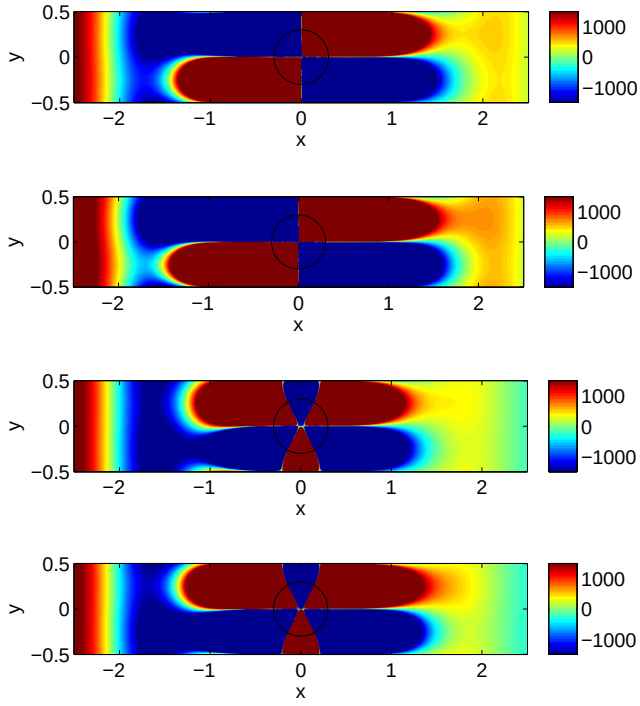

FIG. 7. Wave field patterns (real part of u) of the four asymmetric solutions coupled to the second and third NSWs.

While our main concerns are the solutions for weak incident waves, we also try to track the solutions as the incident amplitude $A^{(i)}$ is increased. In Fig. 8, we show the transmission coefficients as functions of $A^{(i)}$ for seven solutions of the nonlinear diffraction problem at the fixed frequency $\omega L/(2\pi c) = 0.53$. The transmission coefficient is defined as the ratio between the transmitted power and the incident power. The first panel of Fig. 8 shows the transmission coefficients for the symmetric solution (solid

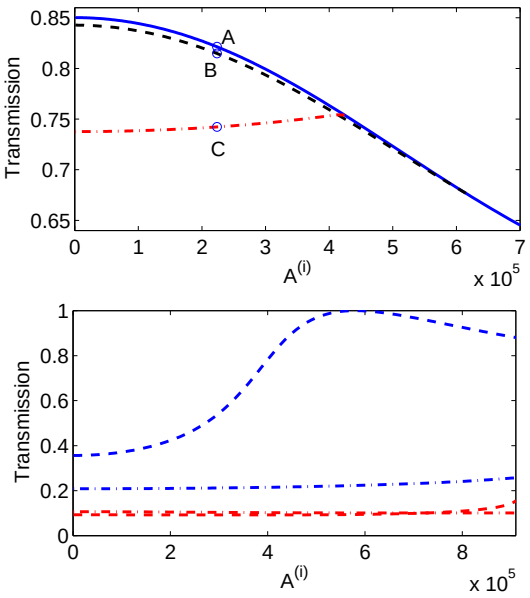

FIG. 8. Dependence of transmission coefficients on incident amplitude $A^{(i)}$ for solutions of the nonlinear diffraction problem at $\omega L/(2\pi c) = 0.53$. Top panel: the symmetric and two asymmetric solutions coupled to the first NSW are shown as the solid, dashed and dash-dot lines, respectively. Bottom panel: asymmetric solutions coupled to the second and third NSWs are shown as the blue and red curves, respectively.

curve) and the two asymmetric solutions (dashed and dash-dot curves) coupled to the first NSW. In the second panel, the blue and red curves correspond to the solutions coupled to the second and third NSWs, respectively.

Our numerical results indicate that the two asymmetric solutions related to the first NSW are merged to the symmetric solution and disappear when $A^{(i)}$ is increased. In Fig. 8 (top panel), the dashed and dash-dot curves have endpoints on the solid curve. This phenomenon is more clearly illustrated in Fig. 9, where a dimensionless

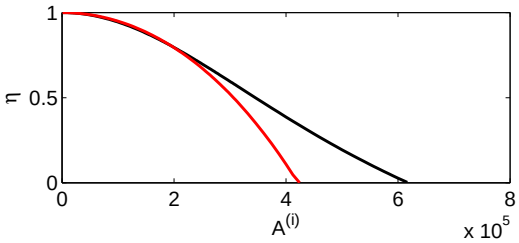

FIG. 9. Measure of asymmetry η for two asymmetric solutions coupled to the first NSW.

quantity η is shown for the two asymmetric solutions. The number η measures the difference between the symmetric solution u_s and an asymmetric solution u_a, and is defined as

$$\eta = \frac{\int_D |u_s - u_a|^2 \mathrm{d}x\mathrm{d}y}{\int_D |u_s|^2 \mathrm{d}x\mathrm{d}y + \int_D |u_a|^2 \mathrm{d}x\mathrm{d}y},$$

where D is the disk of radius a. A small η indicates that u_a is close to u_s, and η equals to zero when the two solutions are identical. In Fig. 9, the blue and red curves correspond to dashed and dash-dot curves in the top panel of Fig. 8, respectively. For each solution, η decreases to zero as the incident amplitude reaches a critical value. To understand the disappearance of the asymmetric solutions better, we need to look at the field patterns for larger $A^{(i)}$. In Fig. 10, we show the wave field patterns of

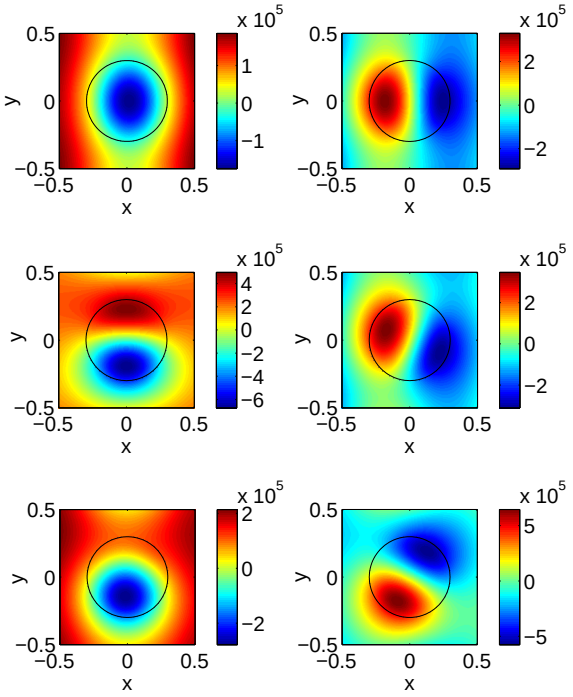

FIG. 10. Wave field patterns, Re(u) in the left and Im(u) in the right, of the three solutions marked as A, B and C in Fig. 8 (top panel), for $A^{(i)} = \sqrt{5} \times 10^5$ V/m and $\omega L/(2\pi c) = 0.53$.

the three solutions marked as A, B and C in the top panel of Fig. 8. It seems that the field patterns of the asymmetric solutions rotate as $A^{(i)}$ is increased, and become symmetric (with respect to the x axis) when they disappear. Asymmetric solutions associated with the second and third NSWs persist as $A^{(i)}$ is increased (at least up to 9×10^5 V/m), probably due to different field patterns between these NSWs and the symmetric solution.

The above solutions are obtained by the numerical method described in Appendix A. Due to the high order of accuracy of the method, our numerical results are obtained using 52 points to discretize the circle at $r = a$, and 26 points to discretize the radial variable r. The solutions are computed by increasing $A^{(i)}$ in small steps, and Newton's method is used as the iterative scheme when $A^{(i)}$ is increased.

VI. CONCLUSION

In this paper, we analyzed the diffraction of plane incident waves by a periodic array of circular cylinders with a Kerr nonlinearity. Through a perturbation analysis and numerical simulations, we found that normally incident plane waves can couple to the NSWs, leading the existence of multiple solutions related to the symmetry breaking phenomenon. Unlike existing studies on optical bistability and symmetry breaking, the asymmetric solutions appear for incident waves of arbitrarily low intensity and for any frequency satisfying $\omega L/(2\pi c) < 1$. Mathematically, our study indicates that the boundary value problem of the nonlinear Helmholtz equation for a periodic structure has no uniqueness for all frequencies. This is very different from the linear case, where non-uniqueness can only happen at a discrete set of frequencies.

The existence of asymmetric solutions for arbitrarily weak incident waves is only possible on an infinite structure such as the periodic array. For any finite structure surrounded by air, there are only resonance modes with finite Q-factors. It is well-known that nonlinear effects can be enhanced by resonances with large Q-factors [4, 14], but on a finite structure, phenomena like symmetry-breaking only appear when the intensity of the incident wave is sufficiently large. The periodic array is different, since the linear standing waves are resonances with infinite Q-factors. In the linear case, a normal incident wave cannot couple to a standing wave due to the different symmetry. But if the incident wave has a small incident angle, it couples to a resonance mode which is close to the linear standing wave, and the solution has a large amplitude on the array [25, 26]. For the nonlinear case, the nonlinear terms breaks the symmetry and makes it possible for the normal incident wave to couple to the NSWs.

In general, the amplitude of a NSW is very large, since it is proportional to $1/\sqrt{\gamma_1}$, thus an asymmetric solution coupled to the NSW has large stored energy, and a switching between the symmetric and asymmetric solutions may be difficult. However, near the frequency ω_* of a linear standing wave, the amplitude of the NSW can be small, since it is proportional to $\sqrt{\omega_* - \omega}$. Therefore, useful applications may be realized for ω near ω_*.

Related to this work, there are a number of important questions. First of all, the stability of the symmetric and asymmetric solutions must be studied. Potential applications are possible only if some asymmetric solutions are stable. Secondly, it is important to know whether there are solutions that are nonperiodic in y or have a period larger than L. If there are solutions that do not satisfy the periodic condition Eq. (3), we also need to study their stability. Finally, the limitation of the nonlinear Helmholtz equation must be analyzed. Even for the ideal 2D periodic structure, the equation is derived assuming the third and higher harmonics can be ignored. It is necessary to understand the effect of this approximation to the asymmetric solutions. These questions will be addressed in our future studies.

ACKNOWLEDGMENTS

National Natural Science Foundation of China (11201508, 11401059); Natural Science Foundation Project of CQ CSTC (cstc2016jcyjA0491); The Research Grants Council of Hong Kong Special Administrative Region, China (CityU 11301914).

APPENDIX A

In Section II, the problem is formulated on the square S. Since the governing equation is nonlinear, an iterative method is needed. To speed up the iterations, it is desirable to further reduce the computational domain. Similar to the case studied in [5], we can reduce the domain to the disk

$$D = \left\{(x, y) : r = \sqrt{x^2 + y^2} < a\right\}. \tag{23}$$

The boundary condition is

$$\frac{\partial u}{\partial r} = \mathcal{B}u + A^{(i)} f(\theta), \quad \text{at} \quad r = a, \tag{24}$$

where $\mathcal{B}$ is an operator, f is a function related to the incident wave but independent of $A^{(i)}$, and θ is the angle variable of the polar coordinate system. It is not possible to write down $\mathcal{B}$ and f analytically, but once the circle Γ (at $r = a$) is discretized, they can be easily calculated. The key idea is to first calculate the so-called Dirichlet-to-Neumann (DtN) operator Λ for the linear Helmholtz equation in $S\backslash\overline{D}$ (the domain inside S and outside D), then combine Λ with boundary conditions (3), (6) and (7) to obtain Eq. (24). The details can be found in [5].

A number of iterative methods can be used to solve the nonlinear Helmholtz equation [34]. Newton's method for Eq. (1) can be written as

$$\begin{aligned} &\mathcal{L}u^{(j+1)} + k_0^2\gamma\left\{2|u^{(j)}|^2u^{(j+1)} + [u^{(j)}]^2\bar{u}^{(j+1)}\right\} \\ &= 2k_0^2\gamma|u^{(j)}|^2u^{(j)}, \end{aligned} \tag{25}$$

where $u^{(j)}$ is the current iteration, $u^{(j+1)}$ is the next iteration to be solved, $\bar{u}$ is the complex conjugate of u, and $\mathcal{L}$ is defined in Eq. (15). When the Jacobian is not singular or ill-conditioned at the solution, the method converges quickly if there is a good initial guess [35]. However, the linear system discretizing Eq. (25) may be singular or near singular for some special initial guesses, then Newton's method becomes numerically unstable and must be avoided. In such a case, we use the modified Newton's method which replaces the constant 2 in Eq. (25) by $\sigma > 2$, i.e.,

$$\begin{aligned} &\mathcal{L}u^{(j+1)} + k_0^2\gamma\left\{\sigma|u^{(j)}|^2u^{(j+1)} + [u^{(j)}]^2\bar{u}^{(j+1)}\right\} \\ &= \sigma k_0^2\gamma|u^{(j)}|^2u^{(j)}. \end{aligned} \tag{26}$$

We discretize Eqs. (25) and (26) on D by a mixed pseudospectral method that uses Chebyshev and Fourier collocation schemes for r and θ, respectively [36]. As shown in our previous works [5, 10, 27], the method is capable of producing accurate solutions with relatively small number of discretization points.

APPENDIX B

For $n_0 = 1$ and $\omega L/(2\pi c) < 1$, α_m (for $m \neq 0$) given in Eq. (4) satisfies $\mathrm{i}\alpha_m = -\rho_m$, where $\rho_m = \sqrt{\beta_m^2 - k_0^2 n_0^2} > 0$. Outside the disk D, ϕ_2 satisfies the linear Helmholtz equation $\mathcal{L}\phi_2 = 0$, thus ϕ_2 can be expanded as Eq. (10) with coefficients $d_m^{\pm}$. This leads to

$$\int_{-\frac{L}{2}}^{\frac{L}{2}} \left[\phi_2 \frac{\partial \bar{\phi}}{\partial x}\right]_{x=\frac{L}{2}} \mathsf{d}y = L(-\mathrm{i}\alpha_0 \bar{b}_0^+ d_0^+ - \sum_{m\neq 0} \rho_m \bar{b}_m^+ d_m^+),$$

$$\int_{-\frac{L}{2}}^{\frac{L}{2}} \left[\bar{\phi} \frac{\partial \phi_2}{\partial x}\right]_{x=\frac{L}{2}} \mathsf{d}y = L(\mathrm{i}\alpha_0 \bar{b}_0^+ d_0^+ - \sum_{m\neq 0} \rho_m \bar{b}_m^+ d_m^+).$$

Since ϕ is an odd function of y, we have $b_0^{\pm} = 0$, thus

$$\int_{-\frac{L}{2}}^{\frac{L}{2}} \left[\phi_2 \frac{\partial \bar{\phi}}{\partial x} - \bar{\phi} \frac{\partial \phi_2}{\partial x}\right]_{x=\frac{L}{2}} \mathsf{d}y = -2\mathrm{i}\alpha_0 \bar{b}_0^+ d_0^+ L = 0.$$

Based on the above equation, a similar equation at $x = -L/2$, and the periodic condition, we get

$$\int_{\partial S} \left[\phi_2 \frac{\partial \bar{\phi}}{\partial \nu} - \bar{\phi} \frac{\partial \phi_2}{\partial \nu}\right] \mathsf{d}s = 0, \tag{27}$$

where ∂S is the boundary of square S, ν is the outward unit normal vector of ∂S. Equation (20) can be obtained if we multiply Eq. (14) by $\bar{\phi}$, integrate on S, perform an integration by parts, and make use of Eq. (27) and the complex conjugate of Eq. (12).

Let $u^{(r)}$ and $u^{(t)}$ be the reflected and transmitted waves, such that $u = u^{(i)} + u^{(r)}$ for $x < -a$ and $u = u^{(t)}$ for $x > a$. They can be expanded as

$$u^{(r)} = \sum_{m=-\infty}^{\infty} R_m e^{\mathrm{i}[\beta_m y - \alpha_m (x+L/2)]}, \quad x < -a,$$

$$u^{(t)} = \sum_{m=-\infty}^{\infty} T_m e^{\mathrm{i}[\beta_m y + \alpha_m (x-L/2)]}, \quad x > a.$$

Multiplying Eq. (1) by $\bar{u}$ and integrating the result on S, we obtain the power balance law:

$$|R_0|^2 + |T_0|^2 = |A^{(i)}|^2. \tag{28}$$

Assuming

$$\phi_1(\pm L/2, y) = \sum_{m=-\infty}^{\infty} c_m^{\pm} e^{i\beta_m y},$$

then Eq. (11) gives

$$T_0 = CA^{(i)} c_0^+ + ...$$
$$A^{(i)} + R_0 = CA^{(i)} c_0^- + ...$$

If Eq. (28) is also expanded in a power series of δ, then the leading term gives

$$|c_0^+|^2 + |c_0^- - \bar{C}|^2 = 1,$$

or

$$|c_0^+|^2 + |c_0^-|^2 - 2\mathrm{Re}(Cc_0^-) = 0.$$

Multiplying Eq. (13) by $\bar{\phi}_1$ and integrating the result on S, we obtain

$$\int_S \left(-|\nabla\phi_1|^2 + k_0^2 n^2 |\phi_1|^2 + 2k_0^2 \gamma |\phi|^2 |\phi_1|^2\right) \mathsf{d}x\mathsf{d}y$$
$$+k_0^2 \int_D \gamma \phi^2 \bar{\phi}_1^2 \mathsf{d}x\mathsf{d}y + \int_{\partial S} \bar{\phi}_1 \frac{\partial \phi_1}{\partial \nu} \mathsf{d}s = 0. \tag{29}$$

It can be verified that

$$\mathrm{Im}\left(\int_{\partial S} \bar{\phi}_1 \frac{\partial \phi_1}{\partial \nu} \mathsf{d}s\right)$$
$$= \alpha_0 L \left[|c_0^+|^2 + |c_0^-|^2 - 2\mathrm{Re}(Cc_0^-)\right] = 0.$$

Thus, the imaginary part of Eq. (29) gives

$$\mathrm{Im}\left(\int_D \gamma \phi^2 \bar{\phi}_1^2 \mathsf{d}x\mathsf{d}y\right) = 0.$$

The above is identical to Eq. (21).

We let ψ and φ satisfy Eqs. (13), (17) and

$$\partial_x \psi = -\mathcal{T}\psi + 2\mathrm{i}\alpha_0, \quad x = -L/2,$$
$$\partial_x \varphi = -\mathcal{T}\varphi + 2\alpha_0, \quad x = -L/2,$$

then $\phi_1 = \cos(d)\psi + \sin(d)\varphi$, and

$$\phi_1^2 = \cos^2(d)\psi^2 + \sin(2d)\psi\varphi + \sin^2(d)\varphi^2.$$

Let K_1, K_2 and K_3 be given by

$$K_1 = \mathrm{Im}\left(\int_D \bar{\phi}^2 \psi^2 \, \mathsf{d}x\mathsf{d}y\right),$$
$$K_2 = \mathrm{Im}\left(\int_D \bar{\phi}^2 \psi\varphi \, \mathsf{d}x\mathsf{d}y\right),$$
$$K_3 = \mathrm{Im}\left(\int_D \bar{\phi}^2 \varphi^2 \, \mathsf{d}x\mathsf{d}y\right),$$

then Eq. (21) gives

$$K_1 \cos^2(d) + K_2 \sin(2d) + K_3 \sin^2(d) = 0.$$

The above can be written as a quadratic equation for $\tan(d)$ or $\cot(d)$, and it can also be reduced to Eq. (22), if we define θ_* and K by

$$K_0 = \sqrt{(K_1 - K_3)^2 + 4K_2^2},$$
$$\cos\theta_* = 2K_2/K_0,$$
$$\sin\theta_* = (K_1 - K_3)/K_0,$$
$$K = -(K_1 + K_3)/K_0.$$

[1] R. W. Boyd, *Nonlinear Optics*, 3rd ed. (Academic, 2008).
[2] H. Gibbs, *Optical Bistability: Controlling Light with Light* (Academic, 1985).
[3] E. Centeno and D. Felbacq, Phys. Rev. B **62**, R7683–R7686 (2000).
[4] J. Bravo-Abad, A. Rodriguez, P. Bermel, S. G. Johnson, J. D. Joannopoulos, and M. Soljacic, Opt. Express **15**, 16161–16176 (2007).
[5] L. Yuan and Y. Y. Lu, Opt. Express **21**, 11952–11964 (2013).
[6] J.P. Torres, J. Boyce, and R.Y. Chiao, Phys. Rev. Lett. **83**, 4293–4296 (1999).
[7] B. Maes, P. Bienstman, and R. Baets, Opt. Express **16**, 3069–3076 (2008).
[8] E. Bulgakov, K. Pichugin, and A. Sadreev, Phys. Rev. B **83**, 045109 (2011).
[9] E. N. Bulgakov and A. F. Sadreev, Phys. Rev. B **84**, 155304 (2011).
[10] L. Yuan and Y. Y. Lu, Opt. Express **22**, 30128–30136 (2014).
[11] B. Maes, M. Soljačić, J. D. Joannopoulos, P. Bienstman, R. Baets, S.-P. Gorza, and M. Haelterman, Opt. Express **14**, 10678–10683 (2006).
[12] F. Diebel, D. Leykam, M. Boguslawski, P. Rose, C. Denz, and A. S. Desyatnikov, Appl. Phys. Lett. **104**, 261111 (2014).
[13] N. C. Panoiu, M. Bahl, and R. M. Osgood, Jr., Opt. Express **12**(8), 1605–1610 (2004).
[14] M. Soljacic and J. D. Joannopoulos, Nat. Mater. **3**, 211–219 (2004).
[15] S. Fan, J. N. Winn, A. Devenyi, J. C. Chen, R. D. Meade, and J. D. Joannopoulos, J. Opt. Soc. Am. B **12**(7), 1267-1272 (1995).
[16] D. N. Chigrin, A. V. Lavrinenko, and C. M. Sotomayor Torres, Opt. Express **12**, 617-622 (2004).
[17] A.-S. Bonnet-Bendhia and F. Starling, Math. Methods Appl. Sci. **17**, 305–338 (1994).
[18] H. D. Maniar and J. N. Newman, J. Fluid Mech. **339**, 309–330 (1997).
[19] D. V. Evans and R. Porter, Q. J. Mech. Appl. Math. **51**(2), 263–274 (1998).
[20] R. Porter and D. V. Evans, Wave Motion **43**, 29–50 (2005).
[21] S. Shipman and D. Volkov, SIAM J. Appl. Math. **67**, 687–713 (2007).
[22] C. W. Hsu, B. Zhen, J. Lee, S.-L. Chua, S. G. Johnson, J. D. Joannopoulos, and M. Soljačić, Nature **499**, 188-191 (2013).
[23] E. N. Bulgakov and A. F. Sadreev, Phys. Rev. A **90**, 053801 (2014)
[24] Z. Hu and Y. Y. Lu, Journal of Optics **17**(6), 065601 (2015).
[25] S. Shipman and S. Venakides, Phys. Rev. E **71**, 026611 (2005).
[26] S. Shipman and H. Tu, SIAM J. Appl. Math. **72**, 216–239 (2012).
[27] L. Yuan and Y. Y. Lu, Opt. Express **23**(16), 20636–20646 (2015).
[28] E. N. Bulgakov and A. F. Sadreev, Phys. Rev. B **81**, 115128 (2010).
[29] E. N. Bulgakov and A. F. Sadreev, Opt. Lett. **39**(17), 5212–5215 (2014).
[30] B. Maes, P. Bienstman, and R. Baets, Opt. Quant. Electron. **36**, 15–24 (2004).
[31] G. Bao, Y. Lia, and H. Wu, J. Comput. Appl. Math., **190**, 170–189 (2006).
[32] G. Baruch, G. Fibich, and S. Tsynkov, J. Comput. Phys. **228**, 3789–3815 (2009).
[33] G. Bao, D. C. Dobson and J. A. Cox, J. Opt. Soc. Am. A, **12**, 1029-1042 (1995).
[34] C. T. Kelley, *Iterative Methods for Linear and Nonlinear Equations* (Society for Industrial and Applied Mathematics, 1995).
[35] A. Griewank, SIAM Review **27**(4), 537–563 (1985).
[36] L. N. Trefethen, *Spectral Methods in MATLAB* (Society for Industrial and Applied Mathematics, 2000).